

Optimization of a Multi-step Model for the Auto-ignition of Dimethyl Ether in a Rapid Compression Machine

Elisa Toulson,[†] Casey M. Allen,[†] Dennis J. Miller,[‡] Harold J. Schock,[†] and Tonghun Lee*[†]

[†]Department of Mechanical Engineering, Michigan State University, 2555 Engineering Building, East Lansing, Michigan 48824, and [‡]Department of Chemical Engineering and Material Science, Michigan State University, 2527 Engineering Building, East Lansing, Michigan 48824

Received March 4, 2010. Revised Manuscript Received April 23, 2010

The research presented here describes the numerical optimization of a multi-step ignition model to predict the auto-ignition of dimethyl ether (DME) in a rapid compression machine. The multi-step modeling concept is aimed at capturing the ignition behavior of new oxygenated fuel blends, where detailed or reduced mechanisms are not available. Experimental data for the ignition of DME/O₂/N₂ mixtures at more than 60 different conditions were used by the optimizer to determine the 26 kinetic parameters of the multi-step model that are unique to each individual fuel or fuel blend. The optimization was performed for conditions with compressed pressures in the range of 10–20 bar, compressed temperatures from 615 to 735 K, and equivalence ratios of 0.43, 0.75, and 1.5. In this region, DME exhibits two-stage ignition behavior. The first and overall ignition delay characteristics predicted by the multi-step model with the DME-optimized constants show good agreement with the experimental data for the majority of conditions tested.

Introduction

The vast quantity of fossil fuels consumed by the transportation sector each year has made it a major contributor to atmospheric pollution and greenhouse gas emissions. Issues with environmental pollution together with concerns for energy security have led to increased research toward more fuel-efficient vehicles and domestically produced alternative and renewable fuels. In particular, plant-derived biofuels are receiving much attention because they are renewable, carbon neutral, and they provide energy security in comparison to their fossil fuel counterparts.^{1,2} Several different liquid and gaseous fuels derived from biomass are being researched for use in the transportation sector.³ These fuels include biodiesel,^{3–6}

bioethanol,^{3,7,8} biomethanol,^{9,10} biohydrogen,^{2,11,12} and bio-syngas-derived Fischer–Tropsch synthesis fuels.^{13–16}

The purpose of the present study is to demonstrate the use of a multi-step model coupled with a genetic algorithm optimization routine for predicting two-stage auto-ignition of oxygenated fuels in a rapid compression machine (RCM), specifically for new oxygenated fuel blends, where detailed or reduced chemical kinetics models are not available. This study is a continuation of previous work,¹⁷ which focused on modifying the multi-step model of Halstead et al.,^{18,19} so that it could be used to predict the auto-ignition of oxygenated fuels. With a multi-step model, the reaction steps are empirical and, consequently, only describe the overall behavior of the detailed kinetics.²⁰ Because of this, the kinetic parameters may require modification if the model is used with different fuels or fuel blends. The overall simplicity of the model drastically cuts down the computation time when incorporated into computational fluid dynamics (CFD) models.

The multi-step model presented here is modified for inclusion of oxygenated fuel compounds and has the flexibility to model complex ignition trends that are impossible to capture using a single global reaction model that is incapable of accommodating both low- and high-temperature regions.^{21,22}

*To whom correspondence should be addressed. Telephone: (517) 432-3187. E-mail: tonghun@msu.edu.

(1) Westbrook, C. K.; Pitz, W. J.; Westmoreland, P. R.; Dryer, F. L.; Chaos, M.; Osswald, P.; Kohse-Höinghaus, K.; Cool, T. A.; Wang, J.; Yang, B.; Hansen, N.; Kasper, T. *Proc. Combust. Inst.* **2009**, *32* (1), 221–228.

(2) Demirbas, A. *Energy Convers. Manage.* **2008**, *49* (8), 2106–2116.

(3) Demirbas, A. *Prog. Energy Combust. Sci.* **2007**, *33* (1), 1–18.

(4) Lapuerta, M.; Armas, O.; Rodríguez-Fernández, J. *Prog. Energy Combust. Sci.* **2008**, *34* (2), 198–223.

(5) Shahid, E. M.; Jamal, Y. *Renewable Sustainable Energy Rev.* **2008**, *12* (9), 2484–2494.

(6) Demirbas, A. *Energy Convers. Manage.* **2009**, *50* (1), 14–34.

(7) Balat, M.; Balat, H. *Appl. Energy* **2009**, *86* (11), 2273–2282.

(8) Gnansounou, E.; Dauriat, A.; Villegas, J.; Panichelli, L. *Bioresour. Technol.* **2009**, *100* (21), 4919–4930.

(9) Hasegawa, F.; Yokoyama, S.; Imou, K. *Bioresour. Technol.* **2010**, *101* (Supplement 1), S109–S111.

(10) Lim, K. O.; Sims, R. E. H. Liquid and gaseous biomass fuels. In *Bioenergy Options for a Cleaner Environment*; Sims, R. E. H., Ed.; Elsevier: Amsterdam, The Netherlands, 2004; Chapter 4, pp 103–140.

(11) Meher Kotay, S.; Das, D. *Int. J. Hydrogen Energy* **2008**, *33* (1), 258–263.

(12) Liu, X.; Ren, N.; Song, F.; Yang, C.; Wang, A. *Prog. Nat. Sci.* **2008**, *18* (3), 253–258.

(13) Tijmensen, M. J. A.; Faaij, A. P. C.; Hamelinck, C. N.; van Hardeveld, M. R. M. *Biomass Bioenergy* **2002**, *23* (2), 129–152.

(14) Jun, K.-W.; Roh, H.-S.; Kim, K.-S.; Ryu, J.-S.; Lee, K.-W. *Appl. Catal., A* **2004**, *259* (2), 221–226.

(15) Takeshita, T.; Yamaji, K. *Energy Policy* **2008**, *36* (8), 2773–2784.

(16) Prins, M. J.; Ptasiński, K. J.; Janssen, F. J. J. G. *Fuel Process. Technol.* **2005**, *86* (4), 375–389.

(17) Toulson, E.; Allen, C. M.; Miller, D. J.; Lee, T. *Energy Fuels* **2010**, *24* (2), 888–896.

(18) Halstead, M. P.; Kirsch, L. J.; Prothero, A.; Quinn, C. P. *Proc. R. Soc. A* **1975**, *346*, 515–538.

(19) Halstead, M. P.; Kirsch, L. J.; Quinn, C. P. *Combust. Flame* **1977**, *30*, 45–60.

(20) Hamosfakidis, V.; Reitz, R. D. *Combust. Flame* **2003**, *132* (3), 433–450.

(21) Sazhina, E. M.; Sazhin, S. S.; Heikal, M. R.; Marooney, C. J. *Fuel* **1999**, *78* (4), 389–401.

(22) Yuan, W.; Hansen, A. C.; Tat, M. E.; Van Gerpen, J. H.; Tan, Z. *Trans. ASAE* **2005**, *48* (3), 933–939.

To predict the combustion process out to the equilibrium state, as required in CFD applications, the multi-step ignition model is coupled with a combustion model, which takes over when combustion is fully initiated [the cell is greater than 1100 K or when a very sharp temperature rise ($> 10^7$ K/s) occurs].^{21,22}

Although the model is targeted for the study of new blends, where kinetic models are not available, for validation purposes, a well-defined compound with information regarding its detailed kinetics is required. In this study, we apply the new model to simulate the ignition behavior of dimethyl ether (DME) and compare the results to data collected in the Case Western Reserve University RCM at a variety of different conditions.^{23,24}

Case Western Reserve University's RCM incorporates a creviced piston to reduce complicated fluid mechanics and near-wall mixing inside the combustion chamber, to improve the post-compression temperature distribution in the combustion chamber and achieve a homogeneous core region and accurate characterization of mixture temperatures for kinetic studies.^{25–27} With RCMs, it is desirable to heat the test fuel mixture as rapidly as possible to a high temperature and pressure with minimal heat losses. For this reason, although the RCM compression time is ~ 30 ms, $\sim 45\%$ of the compression occurs in the last 2 ms (Figure 2), which minimizes the chemistry that occurs during the compression stroke.²⁴ Minimizing the chemistry during this period is important because this reduces the formation of radical species and heat release, which may later affect the ignition delay. Recently, Mittal et al.²⁴ published a RCM kinetic modeling study, in which they indicate that it is important to model the chemistry during the compression stroke, as done in this work, to accurately predict the ignition delay.

Over 60 sets of RCM experimental data for the auto-ignition of DME/O₂/N₂ mixtures were used together with an optimization procedure to determine the 26 kinetic parameters of the multi-level model. The optimization was performed for equivalence ratios of 0.43, 0.75, and 1.5 and for conditions where the pressure and temperature at the end of the RCM compression stroke (or the compressed pressure and compressed temperature) were in the range of 10–20 bar and 615–735 K, respectively. DME exhibits a wide range of ignition behaviors over these regions and is suitable for testing the flexibility of the multi-step model.

There have been several studies that have developed detailed kinetic models of DME pyrolysis and oxidation using experimental data gathered from variable-pressure flow reactors, shock tubes, and jet-stirred reactors, with further validation completed using results from RCMs, counterflow diffusion flames, and premixed, burner-stabilized flames.^{28–31} At the engine-like conditions used in this research, DME has

Table 1. Auto-ignition Reaction Mechanism¹⁹

	step	reaction	rate coefficient
1	initiation	$\text{RH} + \text{O}_2 \rightarrow 2\text{R}^*$	k_{d}
2	propagation	$\text{R}^* \rightarrow \text{R}^* + \text{P} + \text{heat}$	k_{p}
3	propagation	$\text{R}^* \rightarrow \text{R}^* + \text{B}$	$f_1 k_{\text{p}}$
4	propagation	$\text{R}^* \rightarrow \text{R}^* + \text{Q}$	$f_4 k_{\text{p}}$
5	propagation	$\text{R}^* + \text{Q} \rightarrow \text{R}^* + \text{B}$	$f_2 k_{\text{p}}$
6	branching	$\text{B} \rightarrow 2\text{R}^*$	k_{b}
7	termination	$\text{R}^* \rightarrow \text{termination}$	$f_3 k_{\text{p}}$
8	termination	$2\text{R}^* \rightarrow \text{termination}$	k_{t}

been shown to have two-stage, negative temperature coefficient (NTC) auto-ignition properties.²⁴

DME is a promising alternative to petroleum-based fuels because it can be produced from a variety of both renewable and non-renewable sources, including biomass, waste products, natural gas, crude oil, residual oil, and coal.³² DME is the simplest linear ether, with a chemical formula of CH₃OCH₃, has a higher cetane number than conventional diesel, and shows promise for use in compression ignition and homogeneous charge compression ignition (HCCI) engines.^{24,28} In addition, DME has reduced hydrocarbon and carbon monoxide exhaust emissions relative to diesel and almost soot-free combustion because of its chemical structure, which contains no carbon–carbon bonds.^{28,33,34} DME has been shown to have a global warming potential (GWP) of 1.2 over a 20 year time horizon, 0.3 over a 100 year time horizon, and 0.1 over a 500 year time horizon (where by convention the GWP of CO₂ = 1).³⁵ In addition, DME is nontoxic with the overall conclusion that it is environmentally benign.^{30,34,35} The handling properties of DME are similar to liquefied petroleum gas (LPG), therefore enabling the existing LPG infrastructure to be used for transportation, storage, and refueling of DME.^{24,34} The main obstacles of using DME as an engine fuel are associated with its viscosity and lubricity rather than its combustion characteristics. The low viscosity of DME can result in increased leakage in pumps and fuel injectors, while lubrication issues can cause increased wear and eventual failure in these same systems.³⁴

Multi-step Ignition Model

The multi-step kinetics ignition model used for this work is based on the Shell model of Halstead et al.,^{18,19} which was originally designed to predict hydrocarbon auto-ignition (knock) in gasoline engines. More recently, the model has also been shown applicable to diesel and biodiesel ignition in compression ignition engines.^{21,36–39} A detailed description of the application of the multi-step model to oxygenated fuels has been previously reported by the authors,¹⁷ thus, only a brief description is given here.

The model developed by Halstead et al.¹⁹ is shown in Table 1 and consists of seven species (five generic, O₂ and N₂) and eight reactions that are based on the degenerate chain branching characteristic of hydrocarbon auto-ignition. In addition, the

(23) Sung, C. J. <http://www.mae.case.edu/facilities/cdl/projects/rapidcomp/rapiddatabase/dme>, Department of Mechanical and Aerospace Engineering, Case Western Reserve University, Cleveland, OH (accessed on Dec 9, 2009).

(24) Mittal, G.; Chaos, M.; Sung, C.-J.; Dryer, F. L. *Fuel Process. Technol.* **2008**, *89* (12), 1244–1254.

(25) Mittal, G.; Sung, C. J. *Combust. Sci. Technol.* **2007**, *179* (3), 497–530.

(26) Lee, D.; Hochgreb, S. *Combust. Flame* **1998**, *114* (3–4), 531–545.

(27) Brett, L.; Macnamara, J.; Musch, P.; Simmie, J. M. *Combust. Flame* **2001**, *124* (1–2), 326–329.

(28) Curran, H. J.; Pitz, W. J.; Westbrook, C. K.; Dagaut, P.; Boettner, J.-C.; Cathonnet, M. *Int. J. Chem. Kinet.* **1998**, *30* (3), 229–241.

(29) Curran, H. J.; Fischer, S. L.; Dryer, F. L. *Int. J. Chem. Kinet.* **2000**, *32* (12), 741–759.

(30) Fischer, S. L.; Dryer, F. L.; Curran, H. J. *Int. J. Chem. Kinet.* **2000**, *32* (12), 713–740.

(31) Zhao, Z.; Chaos, M.; Kazakov, A.; Dryer, F. L. *Int. J. Chem. Kinet.* **2008**, *40* (1), 1–18.

(32) Arcoumanis, C.; Bae, C.; Crookes, R.; Kinoshita, E. *Fuel* **2008**, *87* (7), 1014–1030.

(33) Kim, M. Y.; Yoon, S. H.; Ryu, B. W.; Lee, C. S. *Fuel* **2008**, *87* (12), 2779–2786.

(34) Semelsberger, T. A.; Borup, R. L.; Greene, H. L. *J. Power Sources* **2006**, *156* (2), 497–511.

(35) Good, D. A.; Francisco, J. S.; Jain, A. K.; Wuebbles, D. J. *J. Geophys. Res.* **1998**, *103* (D21), 28181–28186.

(36) Yuan, W.; Hansen, A. C.; Zhang, Q. Computational study of biodiesel ignition in a direct injection engine. Proceedings of the American Society of Agricultural Engineers (ASAE) Annual International Meeting, Las Vegas, NV, 2003.

(37) Kong, S.-C.; Han, Z.; Reitz, R. D. SAE Tech. Pap. 950278, 1995.

(38) Kong, S.-C.; Reitz, R. D. *J. Eng. Gas Turbines Power* **1993**, *115*, 781–789.

(39) Yuan, W.; Hansen, A. C.; Tat, M. E.; Van Gerpen, J. H.; Tan, Z. *Trans. ASAE* **2005**, *48* (3), 933–939.

model contains 26 constants that are unique to a particular fuel. The species involved in the multi-step model adapted to accommodate oxygenated hydrocarbons are (1) RH, the hydrocarbon fuel of composition $C_nH_{2m}O_k$; (2) O_2 , oxygen; (3) R^* , the radical formed from the fuel; (4) B, the branching agent; (5) Q, the intermediate species; (6) P, the products; and (7) N_2 , nitrogen.

The rate terms f_i ($i = 1, 2, 3$, and 4) are expressed as functions of the fuel and oxygen concentrations as

$$f_i = A_{f_i} \exp\left(\frac{-E_{f_i}}{RT}\right) [O_2]^{x_i} [RH]^{y_i} \quad (1)$$

The kinetic parameters k_i ($i = p_1, p_2, p_3, b$, and t) are in the Arrhenius form

$$k_i = A_i \exp\left(\frac{-E_i}{RT}\right) \quad (2)$$

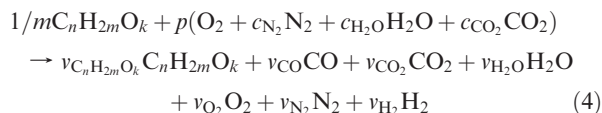
with the exception of k_p , which is given by

$$k_p = \left(\frac{1}{k_{p_1}[O_2]} + \frac{1}{k_{p_2}} + \frac{1}{k_{p_3}[RH]} \right)^{-1} \quad (3)$$

where k_{p_1} , k_{p_2} , and k_{p_3} are the rate coefficients of the rate-determining propagation steps, with the first step first-order in $[O_2]$, the second step unimolecular, and the third step first-order in $[RH]$.

The intermediate species (Q), formed in reaction 4, represent oxygenated compounds, such as aldehydes (RCHO) during the first induction period and alkylperoxy radicals (RO_2) and their isomerization products during the second induction period.³⁷ These intermediate species are capable of enhancing the rate of formation of the degenerate branching intermediate (B) in reaction 5.⁴⁰ The branching intermediate is related to hydroperoxide (RO_2H) at low temperatures and hydrogen peroxide (H_2O_2) at high temperatures.⁴¹

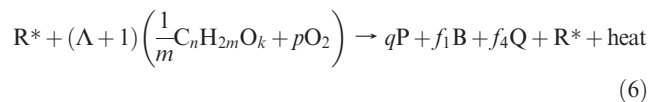
If the fixed CO/CO_2 assumption of the original model is removed and if two hydrogen atoms are abstracted per propagation cycle from the oxygenated hydrocarbon fuel molecule, $C_nH_{2m}O_k$, the main combustion reaction that occurs is



where the oxygen consumption p is

$$p = \frac{(n/m + 1/2 - k/2m)}{\phi} \quad (5)$$

One of the main deficiencies of the original model¹⁹ is that it violates mass conservation. To maintain mass conservation, Schapertons and Lee⁴² modified the propagation sequence, so that the depletion of fuel and oxygen per propagation cycle is increased to account for the production of Q and B, which are generated at rates proportional to the production cycle. To achieve this, the main propagation cycle (reactions 2–4) can be rewritten as



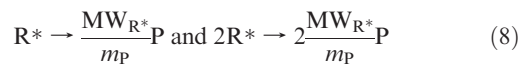
where

$$\Lambda = \frac{f_1MW_B + f_4MW_Q}{MW_{RH}/m + pMW_{O_2}} \quad (7)$$

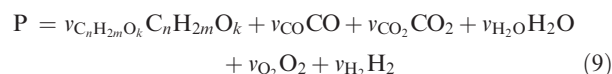
where MW_x is the molecular weight of the species x , p is given in eq 5, and $q = 1 + n/m + p(1 - \phi)$.

The two termination reactions 7 and 8 in Table 1 were also altered to maintain mass conservation by converting radicals into inert species, instead of ignoring their contribution to the mass balance.⁴²

Hamosfakidis and Reitz²⁰ further modified these reactions, so that combustion products were produced from the termination of the radical species. Therefore, reactions 7 and 8 were rewritten as



where the products (P) of the combustion of an oxygenated hydrocarbon are



and m_p is the mass of the combustion products not including N_2 and is equal to

$$\begin{aligned} m_p = & \nu_{C_nH_{2m}O_k}MW_{C_nH_{2m}O_k} + \nu_{CO}MW_{CO} + \nu_{CO_2}MW_{CO_2} \\ & + \nu_{H_2O}MW_{H_2O} + \nu_{O_2}MW_{O_2} + \nu_{H_2}MW_{H_2} \end{aligned} \quad (10)$$

Mass balancing is then accomplished by defining the molecular weights of the generic species as follows:⁴² $MW_{R^*} = (MW_{RH} + MW_{O_2})/2$, $MW_B = 2MW_{R^*}$, and $MW_Q = MW_B$.

Schapertons and Lee's⁴² modified model uses the following equation to calculate temperature, which increases the heat release by a factor of $(\Lambda + 1)$ relative to the original model to account for the increased fuel consumption because of the modification of the propagation cycle

$$\frac{dT}{dt} = \frac{(\Lambda + 1)}{C_v n_{tot}} k_p h V [R^*] \quad (11)$$

where C_v is the constant volume heat capacity, n_{tot} is the total number of moles in volume V , and h is the exothermicity. For the specific value of the CO_2/CO ratio used in Halstead et al.'s model,¹⁹ an exothermicity of 394 kJ/mol is used for primary reference fuels (PRFs). The exothermicity represents the heat release per cycle because of the removal of m^{-1} units of fuel.¹⁹ The exothermicity can be estimated from the heat of formation of the fuel molecule, together with the CO_2/CO ratio of the products, which depends upon the stoichiometry of the reaction. The heat of formation of DME has been calculated to be approximately 184.1 kJ/mol;⁴³ therefore, if the CO_2/CO ratio used in Halstead et al.'s work is kept constant (1:2 CO_2/CO), the exothermicity value of DME is ~ 317 kJ/mol. For this work, the exothermicity was recalculated on the basis of the equilibrium CO_2/CO ratio at the equivalence ratios used. For the lean mixtures ($\phi = 0.43$ and 0.75), an exothermicity value of 442 kJ/mol was used, and for the rich mixture ($\phi = 1.5$), a value of 348 kJ/mol was used.

The concentrations of the species involved in the reactions can be solved by numerically integrating the differential equations for their rates of change. With the modifications suggested by Schapertons and Lee⁴² and Hamosfakidis and Reitz,²⁰ the rate of change of the species concentrations is described by

$$\frac{d[R^*]}{dt} = 2(k_q[RH][O_2] + k_B[B] - k_t[R^*]^2) - f_3k_p[R^*] \quad (12)$$

$$\frac{d[B]}{dt} = f_1k_p[R^*] + f_2k_p[Q][R^*] - k_B[B] \quad (13)$$

$$\frac{d[Q]}{dt} = f_4k_p[R^*] - f_2k_p[Q][R^*] \quad (14)$$

$$\frac{d[O_2]}{dt} = -pk_p[R^*] \quad (15)$$

$$[RH] = \frac{[O_2] - [O_2]_{(t=0)}}{pm} + [RH]_{(t=0)} \quad (16)$$

where $[M]$ is the molar concentration of species M.

(40) Griffiths, J. F. *Prog. Energy Combust. Sci.* **1995**, *21*, 25–107.

(41) Benson, S. W. *Prog. Energy Combust. Sci.* **1981**, *7*, 125–134.

(42) Schapertons, H.; Lee, W. SAE Tech. Pap. 850502, 1985.

(43) Afeefy, H. Y.; Liebman, J. F.; Stein, S. E. In *NIST Chemistry WebBook, NIST Standard Reference Database Number 69*; Linstrom, P. J., Mallard, W. G., Eds.; National Institute of Standards and Technology (NIST): Gaithersburg, MD, 2010; 20899, <http://webbook.nist.gov>.

Table 2. Molar Composition, Equivalence Ratio, Temperature, and Pressure of Simulated Mixtures

ϕ	DME	O ₂	N ₂	T_c (K)	P_c (bar)
0.43	1	7	27	615–723	10, 15
0.75	1	4	30	617–736	10, 15, 20
1.5	1	2	32	618–728	10, 15

With the modifications to the model, it is possible to simulate cool flames, two-stage ignition, and the variation of ignition delay with the temperature. The application of the multi-step model to new fuels can be accomplished by modifying the 26 model constants. The model has been applied to diesel fuel using the model constants suggested by Halstead et al.¹⁹ for PRF 90 but with the adjustment of parameter A_{f4} .^{21,37,44} Hamosfakidis and Reitz also developed a genetic algorithm optimization methodology to determine the parameters for *n*-heptane (C₇H₁₆) and tetradecane (C₁₄H₃₀).²⁰ Recently, suggestions for the constants for the biodiesel surrogate fuel, methyl butanoate, have been published.¹⁷

Heat Loss Model

The RCM ignition modeling was achieved by incorporating the multi-step kinetic model with a heat loss model. Mittal and Sung^{25,45} showed that the results of zero-dimensional modeling based on an approach of effective volume perform well in adequately predicting ignition delay, when there is a well-defined homogeneous adiabatic core within the RCM. Mittal and Sung's^{25,45} method involves first estimating the heat loss by conducting a non-reactive experiment by compressing a non-reactive (inert) mixture with the same specific heat and under the same operating condition as the reactive mixture. The non-reactive pressure results are used to derive the empirical heat loss parameters for the specific heat loss model and to determine the time-dependent effective volume of the core region. This type of heat loss modeling is considered adequate if the simulated and experimental pressure traces for the non-reactive case match. Following this, the reactive experiment can be modeled using the same heat loss parameters. For all of the results presented here, the heat loss parameters specific to each set of initial temperature and pressure conditions used were those reported by refs 23 and 24 for use with their DME experimental results.

Optimization of Model Constants

The optimization objective of the current research was to generate the 26 multi-level model constants that provide the best match between the modeling and experimental pressure traces for the range of initial temperature, pressure, and equivalence ratio conditions shown in Table 2. The optimization method involved minimizing the difference between the modeling and experimental traces, by adjusting the multi-level model constants to minimize the following least-squares objective function:

$$f(t) = \frac{1}{2} \sum_{j=1}^m r_j^2(t) \quad (17)$$

where the residuals (r_j) measure the discrepancies between the predicted model and observed data and are defined as $r_j(t) = y_j - p_j$, $j = 1, 2, \dots, m$, where y_j represents the experimental

pressure data and p_j represents the multi-step model pressure data result for the equivalent point in time (t).⁴⁶

In this research, the optimization method was linked to the multi-step model and the model constants were determined with the use of a genetic algorithm global search optimization method accomplished with the Hierarchical Evolutionary Engineering Design System (HEEDS) software.⁴⁷ Because the characteristics of the design space were unknown, a genetic algorithm global search technique was used to explore the large and complex design space to find a solution. This type of search procedure is based on the evolutionary theory of survival of the fittest; therefore, designs that perform well have a higher probability of surviving to influence future designs.⁴⁷

The optimization procedure begins by first evaluating a set of random designs (chosen within the allowable ranges of each variable). Once the first set of designs is evaluated, a subset including the best design is chosen. During the run, new designs are created through either mutation, where changes are made to one or more variables, or crossover, where variables of two designs are interchanged to create a new population of designs. HEEDS allows for the specification of the number of cycles, the generations per cycle, the population size, and the rates of crossover and mutation. The specification of population size controls the number of designs to be used as parents of new designs. Additionally, the population size together with the mutation and crossover rates determine how many designs are evaluated in each generation.⁴⁷

To maintain a broad range of values possible for each constant, the optimization was divided into three sections: a coarse, low-resolution optimizer (11 possible values within the allowable range), a medium-resolution optimizer (101 possible values), and a refined, higher resolution optimizer (1001 possible values). The coarse optimizer was used to determine the order of magnitude of each parameter, and then the best set of values and one random set from each cycle were passed to the medium-resolution optimizer, whose best set and a random set were then passed to the refined optimizer. The initial values used for the optimization were those suggested by Halstead et al.¹⁹ for PRF 90 and are shown together with the allowable ranges for each constant and the final suggested constants for DME in Table 3. Because of the large number of possible solutions for even a low-resolution run, the values of the last six constants (x_1 , y_1 , x_3 , y_3 , x_4 , and y_4), which are for the reaction order of the species in the rate equations, were kept equal to those for PRF90 because it has been reported that the value of these parameters are arbitrary and that their determination can be done independently once the other parameters have been assigned values.^{19,20} Halstead et al. suggest that a good fit for most fuels can be achieved by setting $x_1 \approx 1$, $y_1 \leq 0$, and $x_3 = y_3 = 0$ and that x_4 and y_4 should be set to sensible parameters and only affect the behavior of the second stage of ignition.¹⁹ The optimization process outlined above was repeated until convergence criteria were met and a suitable solution was attained. The resultant error of the best evaluations of the coarse, medium, and refined optimizers (lines) together with all of the refined optimizer evaluations (points) are shown in Figure 1.

(46) Nocedal, J.; Wright, S. J. *Numerical Optimization*, 2nd ed.; Springer: New York, 2006.

(47) Hierarchical Evolutionary Engineering Design System (HEEDS). HEEDS Professional User's Manual, version 5.2, Red Cedar Technology, East Lansing, MI, 2008; <http://www.redcedartech.com>.

(44) Theobald, M. A. Massachusetts Institute of Technology (MIT), Cambridge, MA, 1986.

(45) Mittal, G.; Raju, M. P.; Sung, C.-J. *Combust. Flame* **2008**, *155* (3), 417–428.

Table 3. Initial Values (PRF 90),¹⁹ Parameter Ranges, and Optimized DME Parameter Values^a

	initial values (PRF 90)	minimum value	maximum value	optimized values for DME
A_{p1}	1.0×10^{12}	1.0×10^9	1.0×10^{15}	4.9×10^{13}
E_{p1}	0	-2.5×10^3	1.0×10^4	6.3×10^3
A_{p2}	1.0×10^{11}	1.0×10^8	1.0×10^{14}	7.0×10^{11}
E_{p2}	1.5×10^4	0	2.0×10^4	1.5×10^4
A_{p3}	1.0×10^{13}	1.0×10^{10}	1.0×10^{16}	1.8×10^{15}
E_{p3}	8.5×10^2	-5.0×10^2	2.5×10^3	1.9×10^3
A_q	1.2×10^{12}	1.0×10^9	1.0×10^{15}	2.0×10^{14}
E_q	3.5×10^4	8.5×10^3	6.0×10^4	3.8×10^4
A_b	4.4×10^{15}	1.0×10^{14}	1.0×10^{20}	2.9×10^{19}
E_b	4.5×10^4	1.0×10^2	7.0×10^4	5.2×10^4
A_t	3.0×10^{12}	2.0×10^5	1.0×10^{15}	3.3×10^{14}
E_t	0	-1.0×10^{-5}	2.5×10^4	8.8×10^3
A_{f1}	7.3×10^{-4}	0	1.0×10^3	9.0×10^1
E_{f1}	-1.5×10^4	-2.5×10^4	-1.0×10^1	-1.0×10^1
A_{f2}	1.8×10^2	1	5.0×10^3	4.0×10^3
E_{f2}	-7.0×10^3	-8.0×10^3	-1	-3.8×10^3
A_{f3}	1.47	0	5.0×10^2	2.7×10^2
E_{f3}	1.0×10^4	1	2.0×10^4	1.6×10^4
A_{f4}	1.88×10^4	1.0×10^2	2.5×10^9	1.5×10^7
E_{f4}	3.0×10^4	1.0×10^2	5.0×10^4	4.5×10^4
x_1	1.0			1.0
y_1	0			0
x_3	0			0
y_3	0			0
x_4	-1.0			-1.0
y_4	0.35			0.35

^a A_i (cm, mol, and s units), E_i (cal/mol), and $R = 1.9872 \text{ cal mol}^{-1} \text{ K}^{-1}$.

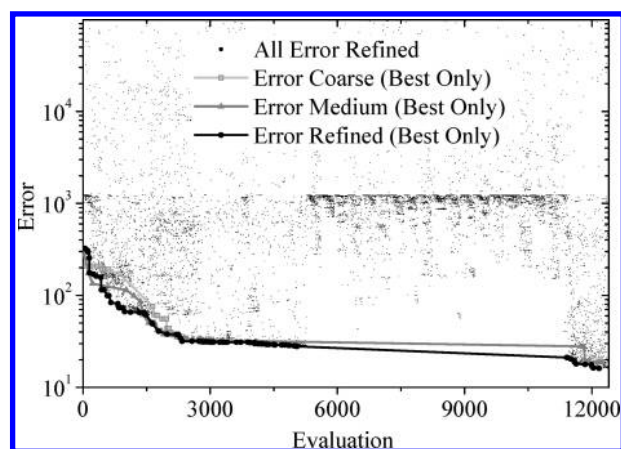


Figure 1. Error between modeling and experimental results. (Lines) Best evaluations for the coarse, medium, and refined optimizers and (points) all of the refined error results.

Results and Discussion

Figure 2 shows a comparison of experimental,²⁴ multi-step modeling and detailed kinetic modeling (models A³¹ and B^{29,30}) pressure traces for the ignition of a DME/O₂/N₂ mixture at $\phi = 0.75$ and a compressed pressure of ~ 15 bar. For this research, ignition delay is defined as the time elapsed from the end of the compression stroke ($t = 0$) to the time where the maximum pressure rise rate occurs. Using this definition, the first and overall ignition delays for the CHEMKIN detailed model B pressure trace are shown in Figure 2.

For each of the modeling traces shown in Figure 2, the same effective volume parameters required for the heat-transfer model, as deduced by Mittal et al.²⁴ for the experimental trace at these conditions, were used. It can be seen from the figure that, prior to ignition, the modeling and experimental traces match well, indicating that the heat-transfer model is satisfactory at these conditions. The detailed kinetic models^{29–31} both overpredict the first-stage (τ_1) and overall (τ_T) ignition delays,

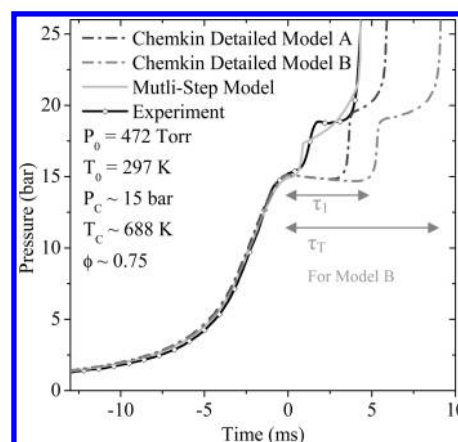


Figure 2. Multi-step model, CHEMKIN detailed models A³¹ and B,^{29,30} and measured²⁴ pressure traces together with definitions of the first-stage and overall ignition delays shown for the CHEMKIN detailed model B case.

while the fitted multi-level model shows good agreement with the experimental data at these conditions. However, the pressure rise that occurs during the first stage of ignition for the experimental results is slightly underpredicted by the multi-step model.

As pointed out by Mittal et al.,²⁴ it is important to properly simulate the compression stroke to correctly simulate the ignition delay, particularly the first stage that occurs during experiments. Mittal et al.²⁴ showed that, although there is little chemical reaction and no measurable effects on the enthalpy of the system during compression, radical initiation begins to occur, which has an effect on the ignition process post-compression. This is especially important for the conditions examined here, because the chemical induction processes have characteristic times that are of the same order of magnitude as the ignition delay.²⁴ Figure 3 shows the RCM effective volume used for the conditions shown in Figure 2, together with the mole fractions of the radical (R*) and intermediate (Q) species calculated with the multi-level model during both

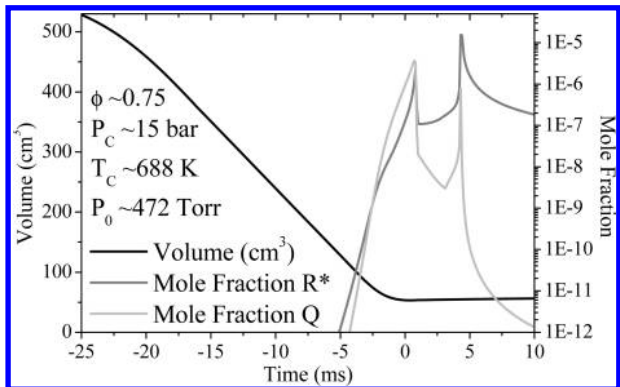


Figure 3. Effective volume of the adiabatic core together with the mole fractions of the radical and intermediate species from the multi-step model for the conditions shown in Figure 2.

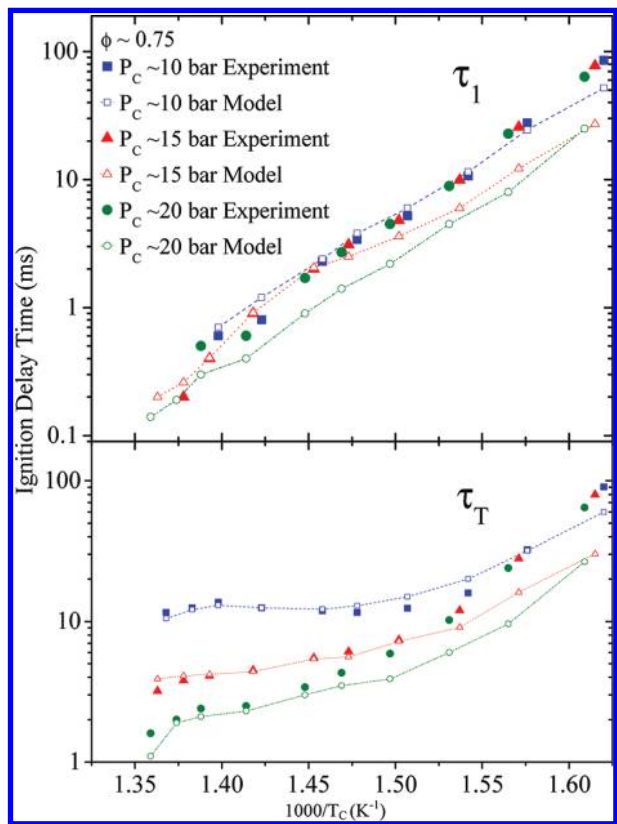


Figure 4. Multi-level model and experimental²⁴ first-stage (upper) and overall (lower) ignition delays at a $\phi = 0.75$ and varying compressed pressures.

compression and ignition of the DME/O₂/N₂ mixture. It can be seen that both species are formed in small amounts prior to the end of compression and that relative maxima exist at the first-stage ignition delay location and again at the overall ignition delay location.

Figures 4–6 show a comparison between the first-stage (upper) and overall (lower) ignition delay results attained with the multi-level modeling (open symbols) and experimental results of Mittal et al.²⁴ (filled symbols) at varying equivalence ratios and compressed pressures as a function of the compressed temperature. Overall, the general trends of the experimental data²⁴ were correctly reproduced with the multi-level model. In Figure 4, which shows the effect of the compressed pressure at $\phi = 0.75$, it can be seen in the bottom portion of

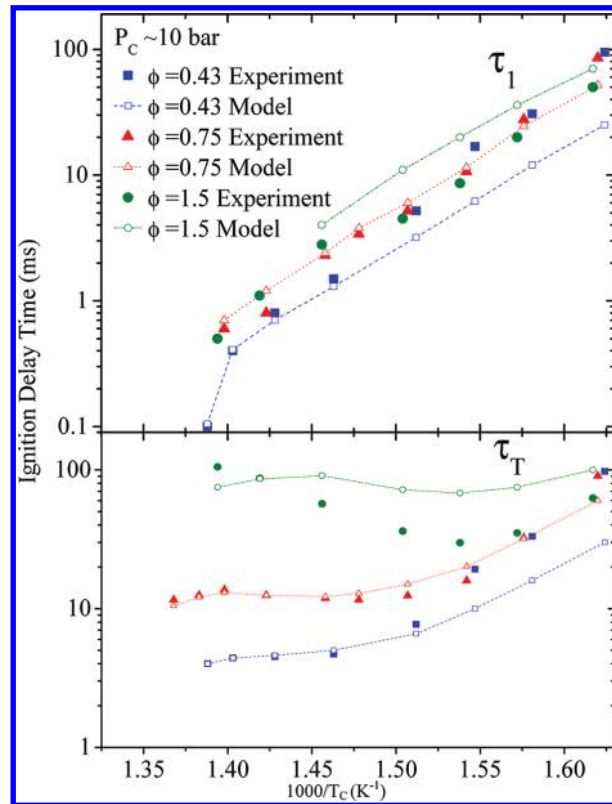


Figure 5. Multi-level model and experimental²⁴ first-stage (upper) and overall (lower) ignition delays at 10 bar compressed pressure and varying equivalence ratios.

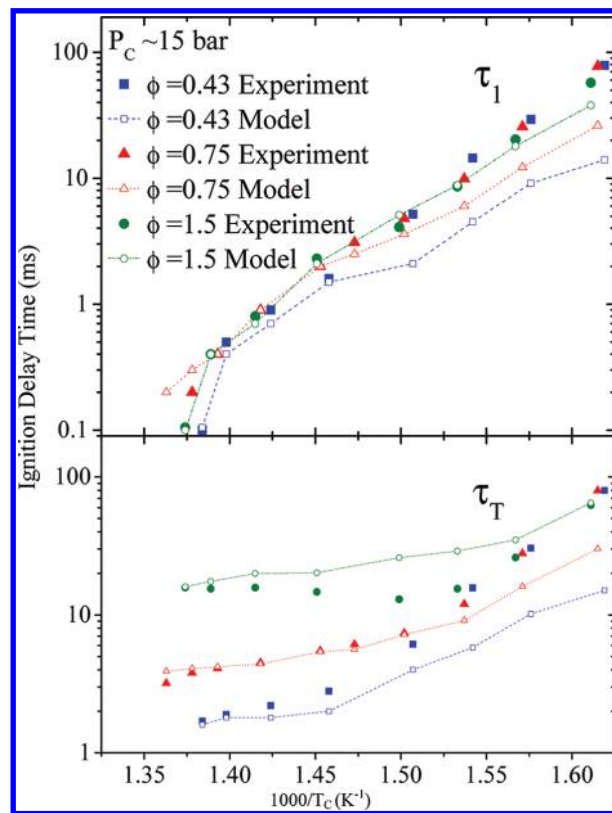


Figure 6. Multi-level model and experimental²⁴ first-stage (upper) and overall (lower) ignition delays at 15 bar compressed pressure and varying equivalence ratios.

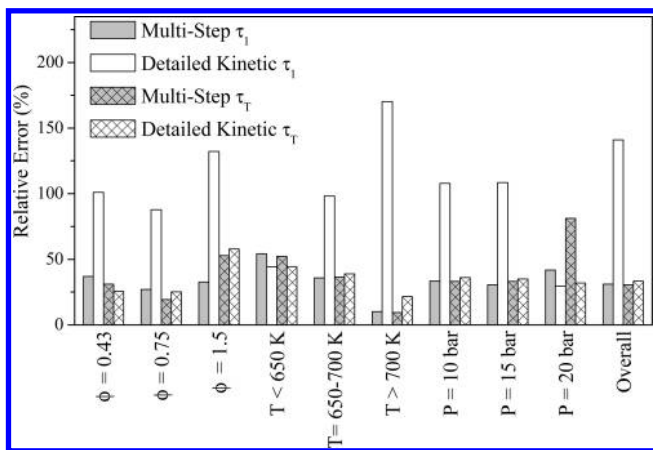


Figure 7. Percent error in the first-stage and overall ignition delays relative to the experimental results²⁴ for the multi-step and detailed kinetic³¹ modeling results.

the figure that, at lower compressed pressures, the NTC behavior becomes significant. It should also be pointed out that, although the experimental data²⁴ showed that the first-stage ignition delay was independent of changes in pressure, with the multi-step model, the first-stage ignition delay was shorter for higher compressed pressures, with the effect more pronounced at lower compressed temperatures.

Figures 5 and 6 show the effect of changes in the equivalence ratio at compressed pressures of 10 and 15 bar, respectively. The first-stage ignition delay is reasonably well-predicted, especially at higher compressed temperatures. The greatest underprediction of the first-stage delay relative to the experimental values occurs at lower compressed temperatures and in leaner mixtures. In addition, the first-stage ignition delay is slightly overpredicted for rich mixtures at the 10 bar compressed pressure condition. Similar to the experimental results, the overall ignition delay predicted by the model increases with an increasing equivalence ratio, especially at higher compressed temperatures. For lower compressed temperatures, the overall delay is less dependent upon the equivalence ratio. This is less convincingly captured in the model. It should be mentioned that, for the cases presented here, the fuel fraction in the overall mixture does not vary and, instead, the ratio of nitrogen/oxygen is altered to achieve the lean and richer mixtures. It is for this reason that the overall ignition delay in the NTC region increases for richer mixtures, which has been attributed to slower branching and reduced peroxy radical formation because of decreased oxygen availability.²⁴

Figure 7 shows the percent relative error in the first-stage and overall ignition delays between the experimental results²⁴ and the multi-step or detailed kinetic³¹ modeling results for the conditions shown in Figures 4–6. In general and particularly for the higher compressed temperature ($T > 700$ K) cases, the multi-step model and experimental data show good agreement. The largest variation between the multi-step modeling and experimental results²⁴ occurs for lower compressed temperatures, higher compressed pressures, and rich mixtures. However, the overall error in the first-stage delay with the multi-level model was less than that obtained with the detailed kinetics,^{29–31} which also show a relatively large error in the first-stage delay, especially for the higher compressed temperature points.

The overall percent relative error between the multi-step modeling and experimental results for both the first-stage and

overall ignition delays was less than 30%. However, it should be noted that the detailed kinetics predicted the first-stage and overall ignition delays more accurately than the multi-level model for compressed temperatures that were less than ~ 650 K and for the 20 bar compressed pressure cases. It is thought that the inferior performance of the multi-step model at lower compressed temperatures may be due to the long experimental ignition delay that occurs, especially for the first stage. In addition, the authors of the original Shell model¹⁹ noted that their model systematically failed to accurately predict the proper behavior of the second stage of ignition as a function of the temperature at low compressed temperatures.

It is anticipated that the accuracy of the multi-level model ignition delay prediction could be improved, especially for the lower compressed temperature conditions, if the multi-level constants were optimized specifically for these conditions. Fitting the multi-step model constants over a wide range of initial conditions can compromise accuracy because of the fact that the model is very simple relative to the complexity of the chemical processes that are used to describe it. Therefore, caution should be used if the DME multi-level model constants shown in Table 3 are used for temperature, pressure, and equivalence ratio conditions outside the range used to calibrate the model constants. Potentially, the model may perform adequately outside the tested range at slightly higher than tested compressed temperatures, lower compressed pressures, and leaner mixtures because the error between the modeling and experimental data is less at these extremes. The multi-step model is most successful at predicting the experimental ignition delay for compressed temperatures greater than 650 K, $\phi = 0.43$ and 0.75, and the 10 and 15 bar compressed pressure cases.

Conclusions

A genetic algorithm optimization was used to determine the kinetic constants in a multi-step combustion model for DME, an oxygenated fuel, such that both the first-stage and overall ignition delay predictions agreed with the experimental RCM results of Mittal et al.²⁴ The optimization was performed for conditions with compressed pressures in the range of 10–20 bar, compressed temperatures from 615 to 735 K, and equivalence ratios of 0.43, 0.75, and 1.5. For these conditions, the overall trends of the experimental data were correctly reproduced with the multi-level model, particularly for the higher compressed temperature cases. The average relative error between the predicted DME ignition delay times of the multi-step model and the experimental results for both the first-stage and overall ignition delays was less than 30%.

It is anticipated that the optimization procedure discussed here could enable the determination of multi-step modeling constants for biofuels and their blends through the use of RCM experimental data. The main benefit of this type of modeling is an enhanced ability to capture the ignition behavior of novel blends of oxygenated compounds, for which no detailed kinetics data are available. The availability of multi-step model constants for a range of oxygenated fuels and blends will be a valuable tool in dramatically reducing the computational time of auto-ignition modeling, especially in CFD applications.

Acknowledgment. This work was preformed under the auspices of the U.S. Department of Energy by Michigan State University under Contract DE-FC26-07NT43278. Additionally, we thank Dr. G. Mittal and Prof. C. J. Sung for allowing us the use of their experimental data.